Re-evaluation of the SRH-parameters for the FeGa defect

Cite as: AIP Conference Proceedings **2147**, 020012 (2019); https://doi.org/10.1063/1.5123817
Published Online: 27 August 2019

Regina Post, Tim Niewelt, Wenjie Yang, Daniel Macdonald, Wolfram Kwapil, and Martin C. Schubert

Re-Evaluation of the SRH-Parameters for the FeGa Defect

Regina Post[1,2,a)], Tim Niewelt[1,2], Wenjie Yang[3], Daniel Macdonald[3], Wolfram Kwapil[1,2] and Martin C. Schubert[2]

[1] *University Freiburg, Department of Sustainable Systems Engineering (INATECH), Emmy-Noether-Str. 2, 79110 Freiburg, Germany*
[2] *Fraunhofer Institute for Solar Energy Systems ISE, Heidenhofstraße 2, 79110 Freiburg, Germany*
[3] *Research School of Engineering, College of Engineering and Computer Science, The Australian National University, Canberra ACT0200, Australia*

[a)]Corresponding author: regina.post@ise.fraunhofer.de

Abstract. In this work the existing SRH parametrizations for the FeGa defect are re-evaluated by a deliberately iron contaminated sample set of varied doping densities. The evolution of the cross-over point is analyzed for this aim, due to its characteristic dependency on the defect parameters of the metastable iron states. It can give insight into the defect parameter, whilst being independent of most factors usually limiting evaluations precision. The proposed parameter adjustment provides an improved description of the measurement data compared to the literature parametrizations.

INTRODUCTION

Iron is a commonly present contamination in silicon and very detrimental for the charge carrier lifetimes in p-type material. Therefore, the assessment of iron contamination levels plays an important role in photovoltaic industrial quality assurance and material evaluation [1]. Luckily an extremely sensitive method to determine the interstitial iron contamination is available based on the metastable character of interstitial iron in p-type silicon. Upon dark storage iron forms pairs with the acceptor dopants, which can be easily dissociated via illumination [2]. Both states the iron-acceptor pairs as well as the isolated interstitial iron (Fe_i), act as recombination active defects for the acceptor being boron, gallium and indium [3]. The recombination activity of iron-boron pairs is well-known and parametrized, since boron is a commonly used acceptor dopant [4]. For gallium as a dopant this is not the case yet.

We have demonstrated in the past that assessment of the iron content is also possible in Ga-doped silicon wafers [5]. However, due to the lack of a suitable parametrization the precision of the evaluation is hampered. In a recent study [5] we were not yet able to provide a better parameterization of iron-gallium pairs (FeGa) due to limitations of the used sample set. This contribution aims to provide a re-evaluation of the existing parametrization of the FeGa state based on investigation of deliberately iron contaminated samples.

EXPERIMENTAL DETAILS

Six Ga-doped Czochralski-grown silicon wafers of different resistivities (0.3 – 3.5 Ωcm) were laser cut into 5x5 cm² pieces. Four samples of each wafer were subjected to a $POCl_3$ diffusion gettering step (785 °C, 1 h) to reduce the iron concentration background. Then the samples were subjected to iron ion implantation at the accelerator facility of the Australian National University at 41keV at room temperature. The ion beam current was controlled with a pico ampere meter and adjusted to a flux of 50 pA. The ion beam was scanned across a 3x3 cm² area on the samples. The implantation dose was defined via the duration of the implantation. The target iron doses were ($8\cdot10^8$, $1.5\cdot10^9$ and $8\cdot10^9$) cm^{-2}, which in a sample of an approximate thickness of 160 µm corresponds to

SiliconPV 2019, the 9th International Conference on Crystalline Silicon Photovoltaics
AIP Conf. Proc. 2147, 020012-1–020012-7; https://doi.org/10.1063/1.5123817
Published by AIP Publishing. 978-0-7354-1892-9/$30.00

average iron concentrations $[Fe]_{implant}$ of ($6\cdot10^{10}$, $1\cdot10^{11}$ and $6\cdot10^{11}$) cm^{-3}, assuming the iron distributes evenly throughout the sample during diffusion. One sample per material was kept as a reference sample. The implantation resulted in a surface-near deposition of the iron atoms. The samples were subjected to an oxidation at 1000 °C for 1 h to drive the iron into the sample. Subsequently the thermally grown oxide layer and the surface-near region that was damaged by the ion bombardment was etched off (20% HF for 1 min, then 40% KOH at 80 °C for 5 min). A 20 nm thick Al_2O_3 layer was deposited using a 180 °C plasma ALD step in an Oxford Instruments OpAL reactor. The passivation was activated via a forming gas anneal at 425 °C for 15 min.

Spatially detection of the introduced iron was performed via iron imaging. This was achieved by the acquisition of photoluminescence (PL) images at low injection densities in the paired and split state. The paired (FeGa) state was achieved via storage in the dark for more than 12 h [5]. The split (Fe_i) state was prepared through exposure to 5 minutes of 790 nm cw laser illumination at an intensity of 2 sun equivalents (note: this corresponds to a photon flux of $5\cdot10^{17}$ photons/cm^2s or 630 W/m^2) [6]. The PL images were calibrated to lifetimes with a self-consistent modulated PL lifetime measurement in the Fe_i-state [7]. Further quasi-steadystate photo-conductance (QSSPC) lifetime measurements in both defect states were performed with a WCT-120 Sinton Instruments Lifetime Tester™. The preparation of both states was again achieved as mentioned above. PL images of the sample were used to ensure that the implanted region was located directly over the measurement coil, whose sensing sensitivity decays rapidly beyond a radius of 15 mm [7]. This ensures that the measured signal is restricted to the implanted region of the samples.

RESULTS AND DISCUSSION

Figure 1 shows two PL-images of the material featuring a resistivity of 1.7 Ωcm. Part (a) shows the non-implanted reference sample of this material and image (b) shows the material with a target implantation dose of $1\cdot10^{11}$ cm^{-3}. The region, where iron was implanted is clearly visible. As mentioned above, the PL images were used to ensure adequate positioning above the QSSPC coil and thereby account for variations in sample placement relative to the ion beam.

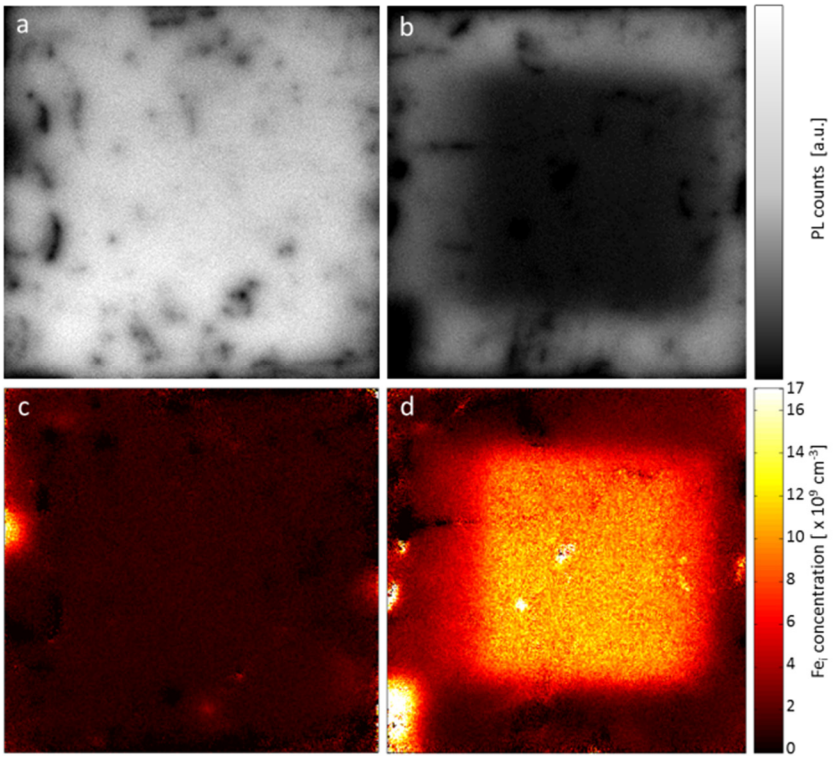

FIGURE 1. PL-images of a Cz-Si:Ga wafer (1.7 Ωcm) without (a) and with (b) an iron implantation region ($[Fe_i]_{target}=1\cdot10^{11}$ cm^{-3}). (c) and (d) show the corresponding Fe-images, displaying the interstitial iron concentration.

The quality of the Shockley-Read-Hall (SRH) parametrizations of both metastable states is crucial for the resulting iron concentration. The parameterization for the Fe_i-state is well established and tested with boron-doped material [8] whilst the parametrization of the FeGa-state is more problematic. Schmidt and Macdonald have determined a parametrization of the FeGa-state based on a sample set of three implanted wafers of different doping densities [3]. However, we have observed disagreement with experimental data in our previous work [5]. Hence we proposed an adjustment of the Schmidt/Macdonald (SM) parametrization using the electron capture cross-section σ_n determined by Ciszek et al. (SMC) via DLTS measurements [9].

Figure 1 (c) and (d) show the result of iron imaging evaluation using the SMC parametrization for the sample shown in Fig. 1 (a) and (b). The implanted region is clearly identified by the increased iron content. The rim of the implanted sample and the non-implanted reference sample overall show low iron concentration $[Fe_i]_{ref,SMC} \approx 1 \cdot 10^9$ cm^{-3} whilst the implanted region shows a much stronger iron concentration of $[Fe_i]_{implant,SMC} = 8 \cdot 10^9$ cm^{-3}. The use of the FeGa parametrization by Schmidt/Macdonald gives the same distribution but higher concentrations ($[Fe_i]_{reference,SM} = 2 \cdot 10^9$ cm^{-3} and $[Fe_i]_{implant,SM} = 1.5 \cdot 10^{10}$ cm^{-3})

Iron evaluation from the QSSPC measurements on the same samples on the other hand, show a reversed trend. The calculated iron concentration resulting from using the SM parametrization is now lower, than the one resulting from SMC: $[Fe_i]_{implant,SM} = 5.5 \cdot 10^9$ cm^{-3} and $[Fe_i]_{implant,SMC} = 3.5 \cdot 10^{10}$ cm^{-3}. This reversed result originates from an experimental difference of the two measurements: the iron imaging is performed well below the cross over point (COP, i.e. the intersection point of the injection dependent lifetime curves of the two states, see e.g. [10] for a detailed explanation), whilst the QSSPC measurements are conducted above the COP (see Fig. 2). In case of a correct parameterization both measurements should result in the same $[Fe_i]$. We observe that neither parameterization fulfills this requirement. This leads to an overestimation of the iron content using SM below the COP (in the iron imaging) and an underestimation above the COP (in the QSSPC-based evaluation) iron determination and vice versa for the SMC parameterization. The observation of this reversing trend is an indicator that the best SRH parametrization can likely be found "between" these existing ones.

The determined $[Fe_i]$ were significantly below $[Fe_i]_{implant}$ for both applied SRH parameterizations for the FeGa defect. While we have just demonstrated flaws in the parameterizations this large discrepancy is likely not merely caused by the applied FeGa defect parameters but an actually lower $[Fe_i]$ than anticipated. One potential reason could be the uncertainty of the implantation process itself. However, the implantation is a well-established process [3,4] and there was no indication of problems during the experiment. An important uncertainty to the actual iron content is given by the drive-in diffusion after implantation. A loss of iron could occur via segregation in the growing oxide (gettering) or in the etched surface region [11]. Also precipitation of iron could occur [11], resulting in iron that is not detectable via lifetime evaluations, since precipitated iron does not take part in the metastable defect state change [12]. Another reason for a lower iron content is gettering in the surface passivation layer [13]. Furthermore, the FeGa complex can exist in two configurations (orthorhombic and trigonal) where one has been suggested to be much less recombination active [14]. The presence of both of these configurations at the same time would lead to an underestimation of the actual iron content. And lastly the parametrization for the Fe_i-state could be unprecise as well, which would also lead to an incorrect determination of the iron content. Overall we cannot easily predict the actual iron concentration a sample should have after implantation. Therefore we chose to not base SRH parameters on the implantation doses. The general trend between different implantation doses should nevertheless remain unaffected, which is reflected in our measurements within each sample sets.

Luckily it is not necessary to know the exact iron concentration to improve the FeGa parametrization because it is possible to exploit another aspect of the iron metastability: The cross over point gives remarkable insight into the defect parameters without a dependence on the absolute iron concentration. Based on the SRH formalism for the Fe_i- and FeGa-state the injection density Δn of the COP can be calculated to:

$$\Delta n_{COP} = \frac{[p_0 + p_1^{FeGa} + k^{FeGa} n_1^{FeGa}] - \left(\frac{\sigma_n^{FeGa}}{\sigma_n^{Fe_i}}\right) \times [p_0 + p_1^{Fe_i} + k^{Fe_i} n_1^{Fe_i}]}{[1 + k^{FeGa}] - \left(\frac{\sigma_n^{FeGa}}{\sigma_n^{Fe_i}}\right) \times [1 + k^{Fe_i}]}$$

It can be seen from eq. (1) that Δn_{COP} does not depend on the iron concentration but only on the SRH-parameters (E_t, k, and σ_n) for the Fe_i- and FeGa-state, the doping density p_0 and the temperature T.

For a given parameter set $\Delta n_{COP}(p_0)$ can differ systematically depend on the used FeGa parameters [10]. For the cases of the SM parametrization (Et= E_v + 0.2 eV , k= 2, $\sigma_{n,SM}$ =4.0·10^{-14} cm^2) and the modified parameter set ($\sigma_{n,SMC}$ =1.2·10^{-14} cm^2) the evaluation of the COP can be seen in Fig. 3. It is visible that for the SM parametrization Δn_{COP} is independent of the p_0, whilst it shifts towards smaller excess carrier densities with decreasing p_0 in the case of the modified parametrization. Since the difference between the two parameter sets consists merely in a different electron capture cross-section σ_n the ratio $\sigma_n^{FeGa}/\sigma_n^{Fei}$ from equation (1) plays a significant role for the general shape of $\Delta n_{COP}(p_0)$. For the SM parameter set $\sigma_n^{FeGa}/\sigma_n^{Fei}$ equals unity, hence Δn_{COP} is independent of p_0. This is not the case for the SMC parametrization, whereby the visible dependence (a decrease in Δn_{COP} for decreasing p_0) is caused. The measured evolution of $\Delta n_{COP}(p_0)$ for the given doping densities in our sample set is ideal to check the FeGa defect parameters.

Figure 2 shows an example of the COP determination conducted in this study. The evaluation is based on lifetime measurements in Fe_i- and FeGa-state measured by the QSSPC. An intersection of the two lifetime curves is clearly observable despite experimental scatter. Linear interpolation was used to determine Δn_{COP}. The statistical scatter of the determined Δn_{COP} was used as estimation for the uncertainty in Δn. This error is affected by measurement noise, different evaluation methods (QSS or transient) and the linear approximation. All determined Δn_{COP} are shown in Fig. 3, as well as the evolution expected from the two parameter sets.

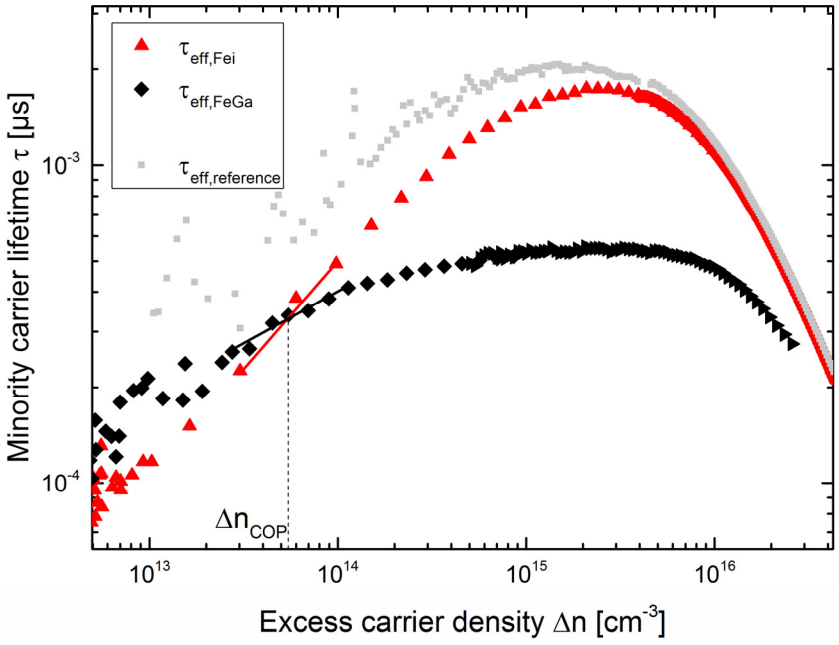

FIGURE 2. QSSPC measurements in the paired FeGa and Fe_i state after illumination for the sample shown in Fig. 1 (b), as well as for the reference sample (Fig. 1 (a)).

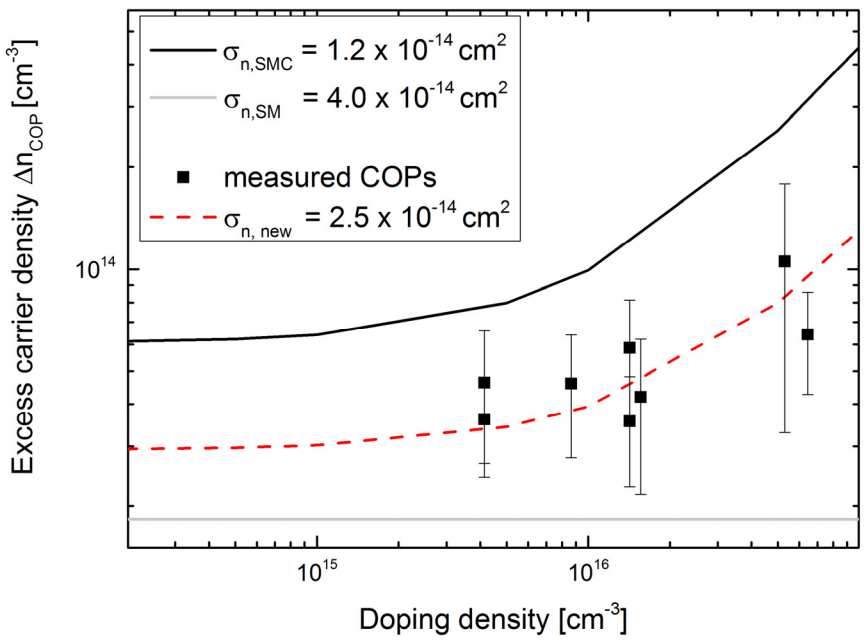

FIGURE 3. Determined Δn_{COP} for samples of varying doping densities. Simulates curves for the evolution of $\Delta n_{COP}(p_0)$ using the energy depth $E_t = E_v + 0.2$ eV and $k = 2$ [3]. The electron capture cross-section σ_n was varied (black: $\sigma_{n,SMC}$, gray: $\sigma_{n,SM}$ and red: $\sigma_{n,new}$).

The evolution of the measured COP supports the observation that both parametrizations SM and SMC are flawed. The visible change in the shape of the COP evolution for the two given parametrizations is caused by the altered σ_n. This and the fact, that the σ_n values found in literature are scattering significantly leads to the approach of adjusting σ_n, while assuming the energy depth E_t and capture cross-section ratio k are correct. A better agreement with the experimental data can be achieved with $\sigma_{n,new} = 2.5 \cdot 10^{-14}$ cm^2.

It should be noted that a change in the capture cross-section for holes σ_p does not show a strong influence, whilst a slight change in E_t affects the shape of the COP evolution drastically as well as the general injection density regime. Adjusting E_t could in turn lead to a better fit to the measured COP as well, but not without a parallel change in σ_n, hence this option is put aside for now.

One indicator, for the quality of the used parameter set is the independence of the evaluated [Fe$_i$]-concentration from the injection density, as discussed above. Evaluation the injection dependent QSSPC measurements the standard deviation from its mean value can be derived. Furthermore the deviation between the mean iron concentration determined by QSSPC measurements $[Fe_i]_{QSSPC}$ and the averaged iron concentration from the implanted area within iron imaging $[Fe_i]_{Fe\text{-}imaging}$ can be given. These standard deviation within the QSSPC iron analysis as well as the deviation between $[Fe_i]_{QSSPC}$ and $[Fe_i]_{Fe\text{-}imaging}$ can be used as an indicator for the quality of the parametrization. The standard deviation for the sample shown in Fig. 2 is 3.5 % using $\sigma_{n,new}$ and the deviation between $[Fe_i]_{QSSPC}$ and $[Fe_i]_{Fe\text{-}imaging}$ is just 8 %. Using the SM parametrization the standard deviation within QSSPC iron analysis equals 7 %, whilst the difference between $[Fe_i]_{QSSPC}$ and $[Fe_i]_{Fe\text{-}imaging}$ reaches 160%. For the SMC parametrization the deviation is even lager with 74 % as the standard deviation within QSSPC determination and the comparison of $[Fe_i]_{QSSPC}$ with $[Fe_i]_{Fe\text{-}imaging}$ yields 78 % difference.

Another option to assess the quality of the proposed parameter set is to test how well a modeled lifetime fits the measurement data. The [Fe$_i$]-concentration determined from the QSSPC measurements is used to calculate the theoretical SRH lifetime curves $\tau_{SRH,Fei}$ and $\tau_{SRH,FeGa}$ (using the according parameter set). These lifetimes are then combined with the non-iron related background lifetime limitation $\tau_{background}$ via inverse addition. The resulting lifetime τ_{model} should represent τ_{eff}. Example curves in comparison to measurement data are shown in Fig. 4. It is visible, that $\tau_{modeled}$ and τ_{eff} coincide approximately, but a still better fit might exist. The same procedure was

repeated for the SM parametrization, as well as for the combined parametrization. Neither of these parameterizations shows an unrealistically strong deviation from the measurements (Fig. 5). Therefore, to be able to compare the three evaluations, the least squares deviation in the injection range of 10^{13} to 10^{16} cm^{-3} was calculated. The determined reduced least square sums are quite large for all three parametrizations. But it was possible to reduce the sum of the least squares to 50% and 20% respectively using $\sigma_{n,new}$. This indicates that this parameter set is the most appropriate one.

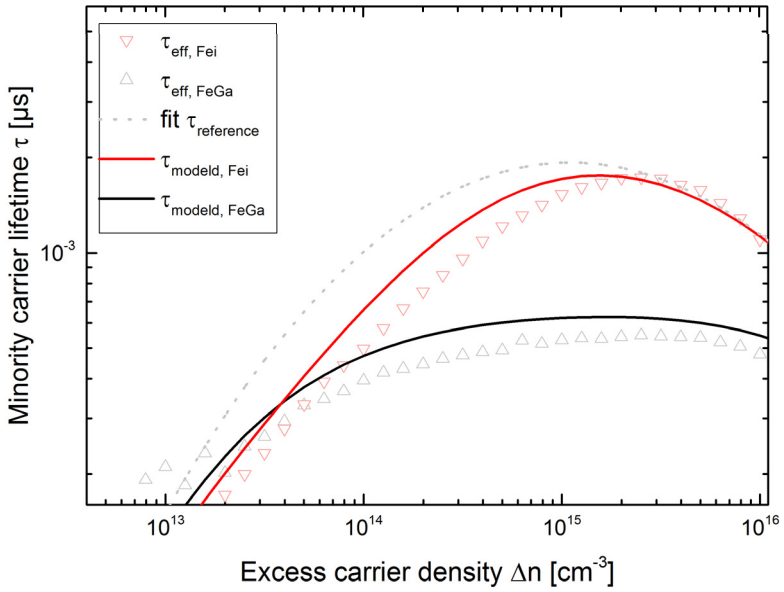

FIGURE 4. Comparison of the determined $\tau_{modeled}$ (using $\sigma_{n,new}$) to the measurement data τ_{eff} in both states. $\tau_{reference}$ determined by an approximation to the measurement of the non-implanted reference sample, which is used as background correction.

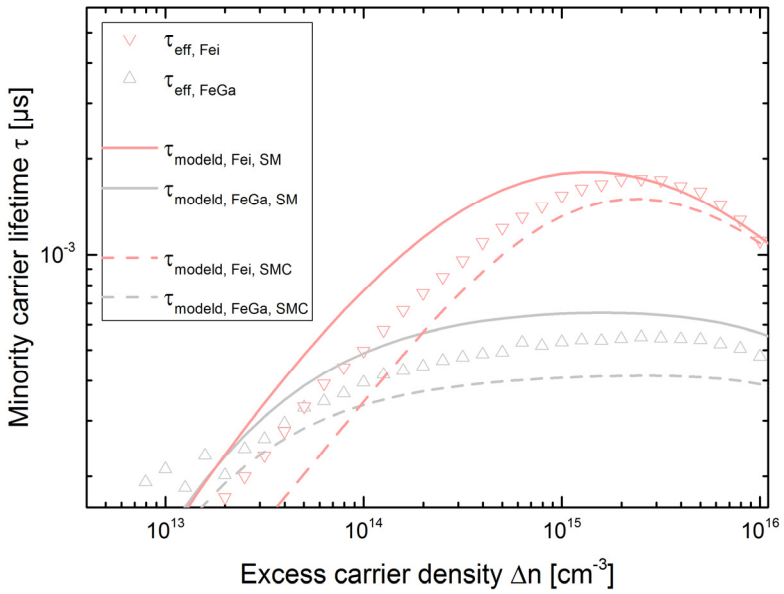

FIGURE 5. Comparison of the determined $\tau_{modeled}$ (using $\sigma_{n,SMC}$ and $\sigma_{n,SM}$) to the measurement data τ_{eff} in both states. The same $\tau_{reference}$ as shown in Fig. 4 is used.

Evaluating both above mentioned criterions on further samples with differing doping densities shows a similar trend. The modeled lifetime curves, corresponding to the ones shown in Fig. 4, do describe the measurements approximately, with the least deviation for the here new chosen $\sigma_{n,new}$. But again the deviations are still significant and it would be desirable to minimize those even further. Also the deviation between the differently determined iron concentrations are minimized with $\sigma_{n,new}$ but for some samples these deviations are significantly larger than for the exemplary presented sample (up to 40% deviation between $[Fe_i]_{QSSPC}$ with $[Fe_i]_{Fe\text{-}imaging}$ using $\sigma_{n,new}$).

CONCLUSION

An improvement for the existing SRH parametrization of the FeGa defect was given, resulting in a reasonable agreement between measured lifetime data and calculated expectation value. Further it was shown, that the adjusted $\sigma_{n,new}$ generates an improved description of the measurement data over a sample set with varied doping densities. Further improvement of the parametrization for the FeGa state, tuning more than just the σ_n could lead to a further reduction of measurement uncertainty in iron evaluation in Ga-doped silicon. To this end the evolution of Δn_{COP} over a varied doping density as well as over a changing temperature range is a promising and powerful tool. This method could also bring along a further improvement for the Fe_i parametrization by [8].

ACKNOWLEDGMENT

This work was supported by the German Federal Ministry for Economic Affairs and Energy (BMWi) and by the industry partners within the research cluster LIMES under contract numbers 0324204A and 0324204C.

The cooperation of Fraunhofer ISE and ANU was supported by the German Federal Ministry of Education and Research (BMBF) within the german-australian research cooperation cluster CCPV under contract number 01DR17019.

The authors would like to thank Dr. C. Sun from ANU for sample preparation and experimental support.

REFERENCES

1. M. C. Schubert, J. Schön, B. Michl, A. Abdollahinia, and W. Warta, "Modeling distribution and impact of efficiency limiting metallic impurities in silicon solar cells," in *38th IEEE Photovoltaic Specialists Conference Austin* (2012), p. 286.
2. D. Macdonald, T. Roth, P. N. K. Deenapanray, K. Bothe, P. Pohl, and J. Schmidt, Journal of Applied Physics **98**, 83509 (2005).
3. J. Schmidt and D. Macdonald, Journal of Applied Physics **97**, 113712 (2005).
4. D. Macdonald, J. Tan, and T. Trupke, Journal of Applied Physics **103**, 73710 (2008).
5. R. Post, T. Niewelt, J. Schön, F. Schindler, and M. C. Schubert, Phys. Status Solidi (a) **121**, 1800655 (2019).
6. M. C. Schubert, H. Habenicht, and W. Warta, IEEE J. Photovoltaics **1**, 168 (2011).
7. J. A. Giesecke, M. C. Schubert, B. Michl, F. Schindler, and W. Warta, Solar Energy Materials and Solar Cells **95**, 1011 (2011).
8. A. A. Istratov, H. Hieslmair, and E. R. Weber, Applied Physics A: Materials Science & Processing **69**, 13 (1999).
9. T. F. Ciszek and T. H. Wang, Journal of Crystal Growth **237-239**, 1685 (2002).
10. D. Macdonald, T. Roth, P. N. K. Deenapanray, T. Trupke, and R. A. Bardos, Appl. Phys. Lett. **89**, 142107 (2006).
11. J. D. Murphy, R. E. McGuire, K. Bothe, V. V. Voronkov, and R. J. Falster, J. Appl. Phys. **116**, 53514 (2014).
12. G. Zoth and W. Bergholz, Journal of Applied Physics **67**, 6764 (1990).
13. A. Y. Liu and D. Macdonald, Appl. Phys. Lett. **110**, 191604 (2017).
14. T. U. Nærland, S. Bernardini, H. Haug, S. Grini, L. Vines, N. Stoddard, and M. Bertoni, Journal of Applied Physics **122**, 85703 (2017).